Journal of Alloys and Compounds 489 (2010) 552–557

Contents lists available at ScienceDirect

Journal of Alloys and Compounds

journal homepage: www.elsevier.com/locate/jallcom

Pulverization mechanism of the multiphase Ti–V-based hydrogen storage electrode alloy during charge/discharge cycling

Mingxia Gao*, Shengcai Zhang, He Miao, Yongfeng Liu, Hongge Pan

Department of Materials Science and Engineering, Zhejiang University, Hangzhou 310027, China

ARTICLE INFO

Article history:
Received 1 August 2009
Received in revised form
13 September 2009
Accepted 15 September 2009
Available online 25 September 2009

Keywords:
Metal hydride
Electrochemical reaction
Microstructure
Pulverization

ABSTRACT

Pulverization is an important key factor for the electrochemical cycle stability of many hydrogen storage alloys. In this paper, the pulverization mechanism of the multiphase Ti–V-based hydrogen storage alloy which mainly consists of a V-based solid solution phase with the BCC structure and a C14 Laves phase is studied based on a sample material of the $Ti_{0.8}Zr_{0.2}V_{2.7}Mn_{0.5}Cr_{0.6}Ni_{1.25}Fe_{0.2}$ alloy. The microstructure of the alloy and the morphology change of the alloy electrode during the charge/discharge process were observed by transmission electron microscope, scanning electron microscope and atomic force microscope, etc. The effect of mechanical properties of the V-based phase and the C14 Laves phase on the pulverization behavior of the Ti–V-based alloy is discussed. The results show that microcracks initially occur at the phase boundary of the V-based phase and the C14 Laves phase and then extend to the C14 Laves phase in the charge/discharge process. The phase boundary is composed of a Ti segregated amorphous layer with a thickness of about 90 nm, mismatching with the crystallized V-base phase and C14 Laves phase. The toughness of the C14 Laves phase is much lower and the hardness is higher than that of the V-based phase. The weak bonding strength of the phase boundary, the lower toughness of the C14 Laves phase and the large volume expansion/contraction of the C14 Laves phase during charge/discharge cycling are the main factors that cause the pulverization of the Ti–V-based alloy.

1. Introduction

As an environmentally compatible and regenerative secondary energy, Ni/MH (nickel/metal hydride) battery has been widely used in small portable electronic devices. However, the theoretical capacity of the most commercially used negative electrode materials of Ni/MH batteries, AB_5 type hydrogen storage alloys, is only around 320 mAh/g, which cannot meet fully the increasing demand of the application of Ni/MH batteries for high power devices, such as the electric tools of medium-sized and even big-sized, electric bicycles, hybrid vehicles, etc. Investigations of new negative electrode materials for Ni/MH batteries of high capacity, good kinetics and long cycle life have never stopped. A series of high capacity multiphase hydrogen storage electrode Ti–V-based alloys which mainly consist of a V-based solid solution BCC (body centered cubic) phase as the main hydrogen absorption phase and a network of TiNi BCC phase or C14 Laves phase as the secondary phase of electro-catalyst and micro-current collector have been developed since the end of the last century [1–5]. However, their poor cycle stability is the main obstacle for their practical application. Studies on the improvement of their overall electrochemical properties have been widely investigated and progress has been made. Previous studies showed that multi-alloying Ti–V-based alloys with suitable transitional elements [6–11], heat treatment [12–13] as well as rapid solidification fabrication method [14] are effective ways to improve the cycling stability of the Ti–V-based alloys.

The cycling stability of hydrogen storage alloys is complexly affected by many factors. It is well accepted that the pulverization of the alloy particles caused by the lattice expansion/contraction due to hydride formation/decomposition and the oxidation/corrosion of the active components are two main factors responsible for the capacity degradation of the Ti–V-based alloys [15–19]. For examples, the improvement of the cycling stability of the $Ti_{0.8}Zr_{0.2}V_{0.5}Mn_{0.5-x}Cr_xNi_{0.8}$ (x = 0–0.5) alloy electrodes by the partial substitution of Cr for Mn is taken as the low pulverization rate and high surface stability of the alloy electrode [6]. An increase of the pulverization property of a Ti–V-based alloy caused by a heat treatment is also reported can improve the cycle stability of the alloy [12]. Moreover, the pulverization accelerates inevitably the oxidation/corrosion of the active components and makes the capacity degradation severe due to the increase of the surface area of the alloy particles.

Pulverization is an important key factor that affects the cycle stability for many kinds of Ti–V-based alloys. However, less attention has been paid to its mechanism [19]. It is thought that to under-

* Corresponding author. Tel.: +86 571 8795 2615; fax: +86 571 8795 2615.
E-mail address: gaomx@zju.edu.cn (M. Gao).

0925-8388/$ – see front matter © 2009 Elsevier B.V. All rights reserved.
doi:10.1016/j.jallcom.2009.09.107

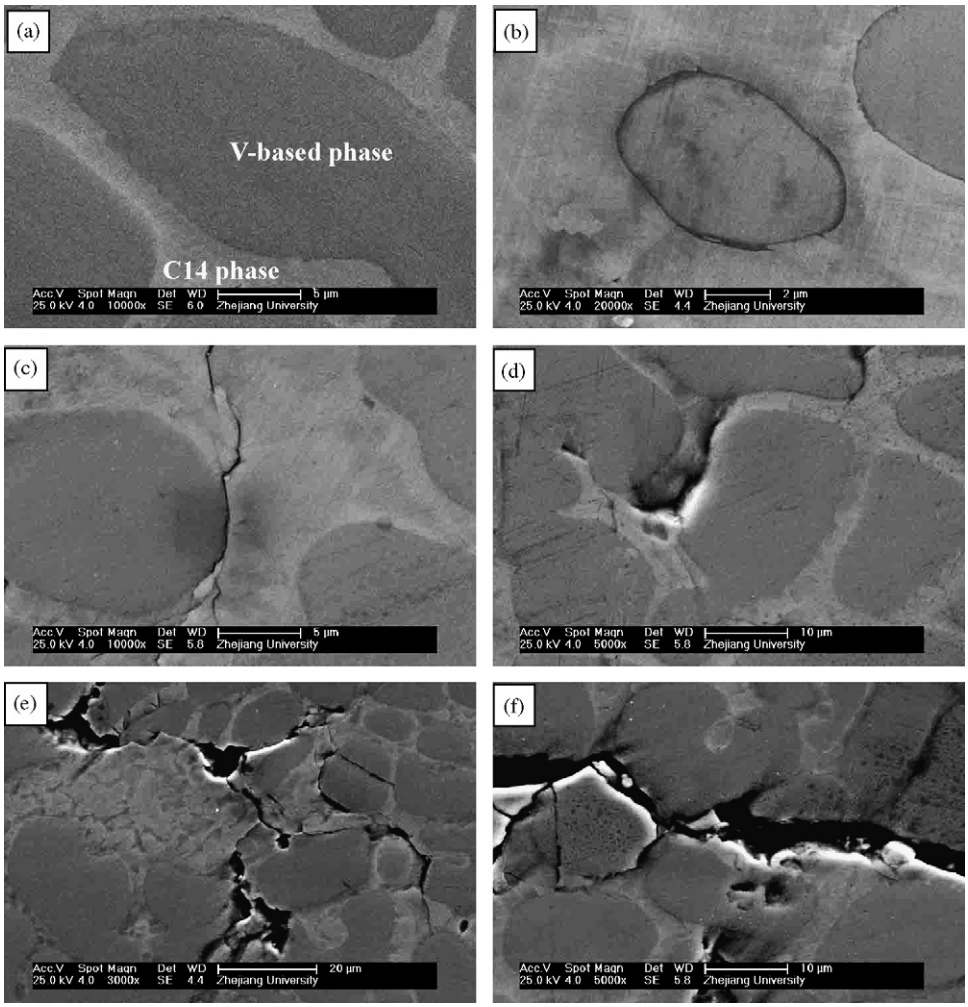

Fig. 1. SEM images of the starting $Ti_{0.8}Zr_{0.2}V_{2.7}Mn_{0.5}Cr_{0.6}Ni_{1.25}Fe_{0.2}$ alloy (a) and of the alloy electrode after charge/discharge process on 36% SOC (b), 72% SOC (c), 108% SOC (d), 144% SOC (e), and 180% (f).

stand the pulverization mechanism is helpful for effectively finding ways to suppress the pulverization and further improving the cycle stability of the Ti–V-based alloys.

In our previous study [11], hydrogen storage alloys of $Ti_{0.8}Zr_{0.2}V_{2.7}Mn_{0.5}Cr_{0.8-x}Ni_{1.25}Fe_x$ ($x = 0.0$–0.8) were investigated with the purpose of developing Fe containing Ti–V-based alloys. In this case the Ti–V-based alloys can be made by partially using V–Fe alloy instead of pure V, and hopefully the cost of the alloys can be reduced, as the former is much cheaper than the latter. Moreover, suitable amount of Fe addition is found profitable on the overall electrochemical properties of the alloy. In the present study, the $Ti_{0.8}Zr_{0.2}V_{2.7}Mn_{0.5}Cr_{0.6}Ni_{1.25}Fe_{0.2}$ alloy, which provides a moderate electrochemical property [11], is selected as the sample material on the purpose of clarifying the pulverization mechanism of the Ti–V-based alloys. The key factors that affect the pulverization behavior of the electrode alloy are discussed.

2. Experimental

The preparation of the $Ti_{0.8}Zr_{0.2}V_{2.7}Mn_{0.5}Cr_{0.6}Ni_{1.25}Fe_{0.2}$ alloy was the same as reported in our previous study [11]. In order to clarify the failure mode of the alloy during the charge and discharge process, an alternative method was applied in the present study. Instead of the normal hydrogen storage alloy electrode for Ni/MH battery that alloy powder mixed with nickel powder are used as the electrode, bulk alloy slice was used as the electrode directly. In this case, the morphology evolution caused by the absorption and desorption of hydrogen during the charge and discharge process can be clearly observed. Alloy slice of dimension of around 7.0 mm × 3.0 mm × 0.7 mm (about 820 mg) was cut from the ingot by an electro-discharge machine and then mechanically polished for the use as the electrode. Charge/discharge tests were carried out in a standard tri-electrode cell, consisting of a working electrode (the testing electrode of the alloy slice), a sintered $Ni(OH)_2$/NiOOH counter electrode and a Hg/HgO reference electrode with a galvanostatic method. The alloy electrode was charged at a current of 100 mA/g for different durations of 60–300 min, corresponding to a state of charge (SOC) of 36–180% (taking charge to its maximum capacity of 340 mAh/g as 100% SOC), followed by a 10 min break, and then discharged at 60 mA/g to a cut-off potential of −0.6 V vs. the Hg/HgO reference electrode.

After the charge/discharge cycle, the alloy electrode was washed by distilled water and then observed by a scanning electron microscope (SEM) and atomic force microscope (AFM: STI 3800N). Element distribution in different phases of the alloy electrode after the charge/discharge process was detected by energy dispersive spectroscopy (EDS) by using SEM. Transmission electron microscope (TEM, JEM-2010HR) was used to observe the phase boundary of the V-based BCC phase and the C14-based Laves phase of the alloy. The chemical compositions of the two phases and the phase boundary were measured by EDS by using TEM. To understand the correlation of the pulverization behavior of the bulk alloy and the mechanical property of the two phases, two simulative alloys with the respective composites of the V-based phases and the C14 Laves phase obtained by EDS by using TEM were prepared with the same induction levitation melting method as for the Ti–V-based alloy. These two alloys are simply named as "V-based alloy" and "C14-based alloy", respectively. The phase identification of the two alloys as well as the $Ti_{0.8}Zr_{0.2}V_{2.7}Mn_{0.5}Cr_{0.6}Ni_{1.25}Fe_{0.2}$ alloy was carried out by X-ray powder diffraction (XRD, Thermo ARL X' TRA), using Cu $K\alpha$ radiation ($\lambda = 1.54$ Å) with a step interval of 0.02° and a count time of 1 s per step. Toughness and hardness of the V-based BCC phase and the C14-based Laves phase were estimated via the "V-based alloy" and the "C14-based alloy" by a Vickers indentation method, in which a diamond pyramid indenter and a load of 49 N were used.

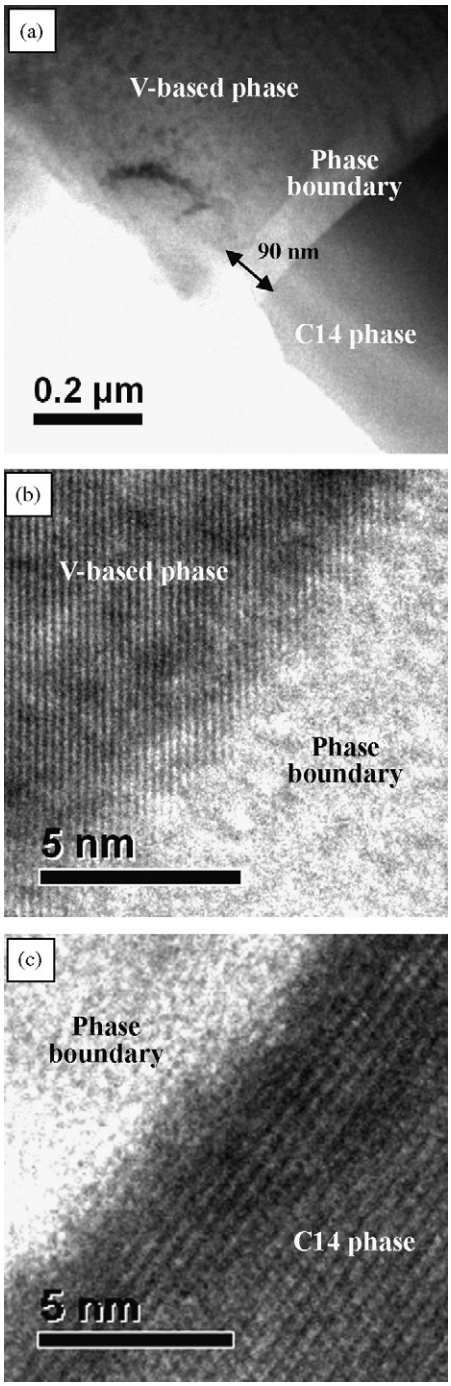

Fig. 2. TEM image (a) and HRTEM images of the phase boundary adjoining to the V-based phase (b), and the C14 Laves phase (c) of the $Ti_{0.8}Zr_{0.2}V_{2.7}Mn_{0.5}Cr_{0.6}Ni_{1.25}Fe_{0.2}$ alloy.

3. Results and discussion

The $Ti_{0.8}Zr_{0.2}V_{2.7}Mn_{0.5}Cr_{0.6}Ni_{1.25}Fe_{0.2}$ alloy is composed of a V-based BCC phase with a dendritic structure and a C14 Laves phase in a three-dimensionally network in between the V-based dendritic phase [11]. Fig. 1(a) is a SEM micrograph of the starting $Ti_{0.8}Zr_{0.2}V_{2.7}Mn_{0.5}Cr_{0.6}Ni_{1.25}Fe_{0.2}$ alloy. Fig. 1(b)–(f) displays the formation and propagation of the cracks in the alloy electrode during the charge/discharge process with the increase of the charge duration to different SOC. It can be seen obviously that the cracks widen and propagate with the increase of the SOC from 36% to 180%. For the alloy electrode charged to 36% SOC, microcracks are only found at the phase boundary of the V-based phase and the C14 Laves phase, as displayed in Fig. 1(b). With the charge duration increasing to 72% SOC (Fig. 1(c)), the microcrack extends from the phase boundary to the C14 Laves phase. Cracks further broaden and wide gaps form both in the C14 Laves phase and at the phase boundary of the alloy with the SOC increasing to 108–180% (Fig. 1(d)–(f)). Additionally, crack is sporadically found inside the V-based BCC phase and is always very narrow as shown in Fig. 1(f), which is very different from the wide cracks occurring in the C14 Laves phase and at the phase boundary.

Table 1
Compositions of the C14 Laves phase, the V-based BCC phase and the phase boundary of the $Ti_{0.8}Zr_{0.2}V_{2.7}Mn_{0.5}Cr_{0.6}Ni_{1.25}Fe_{0.2}$ alloy detected by EDS under TEM.

Detected area	Composition (at.%)						
	V	Ti	Ni	Cr	Mn	Fe	Zr
C14 phase	14.6	26.0	39.5	2.8	7.6	3.4	6.1
V-based phase	63.5	3.8	5.2	11.9	11.0	4.7	0.0
Phase boundary	2.8	89.9	2.0	0.6	0.0	0.0	4.8

Pan et al. [17] have revealed that the C14 Laves phase is hydrogenated rather quickly and exhibits much larger unit cell volume expansion/constriction than the V-based BCC phase during charge/discharge cycling. They also reveal that the C14 Laves phase has good electrochemical activity on its surface, decomposing water into hydrogen atoms and OH^- ions and thereby absorbing hydrogen. The unit cell volume increment of the C14 Laves phase reaches more than 30 times than that of the V-based phase during cycling. Moreover, the C14 Laves phase absorbs hydrogen prior to the V-based phase in the charge process. Only when the C14 Laves phase has been hydrogenated to a certain extent, the V-based phase starts to absorb hydrogen from the surface of the C14 Laves phase and gets hydrogenation. So, it can be inferred that the strain formed in the C14 Laves phase cannot be released timely. This should be one of the important reasons that cracks formed and propagated in the C14 Laves phase preferably. That one phase is hydride prior to another not only occurs in the Ti–V-based hydrogen storage alloys but also in the La–Mg–Ni-based multiphase alloys. For instance, the $LaNi_5$ phase was firstly hydrided in the very initial electrochemical charge process [20].

Fig. 2(a) shows the TEM image of the phase boundary of the V-based phase and the C14 Laves phase of the $Ti_{0.8}Zr_{0.2}V_{2.7}Mn_{0.5}Cr_{0.6}Ni_{1.25}Fe_{0.2}$ alloy. The thickness of the boundary is about 90 nm. Fig. 2(b) and (c) shows the high resolution TEM (HRTEM) images of the boundary adjoining to the V-based phase and the C14 Laves phase, respectively. It is seen that the phase boundary is composed of a disordered phase, and the V-based phase and the C14 Laves phase show ordered crystal structures. Such incoherent interface normally has high interface energy and offers low bonding strength. The composition of the V-based phase, the C14 Laves phase and the phase boundary detected by EDS are listed in Table 1. As seen from Table 1, the concentration of Ti in the phase boundary is as high as 90 at.%, which is much higher than that of the C14 Laves phase and V-based phase. High segregation of Ti at the grain surface of the Laves phase alloy is reported caused a high oxidation/corrosion in the alkaline solution during the cycling [21]. Moreover, Ti is found tending to segregate and be oxidized at the surface of the C14 Laves phase [16,21]. Thus, it is believed that the severe segregation of Ti extra weakened the bonding strength of the boundary during the charge/discharge process. Moreover, the Ti segregated boundary is also an obstacle for the hydrogen to transfer from the C14 Laves to the V-based BCC phase, decreasing the diffusion rate of the hydrogen from the surface of the C14 Laves phase to the V-based phase. Thus, with the increase of the charge state, more amount of hydrogen gathered in the C14 Laves phase, causing

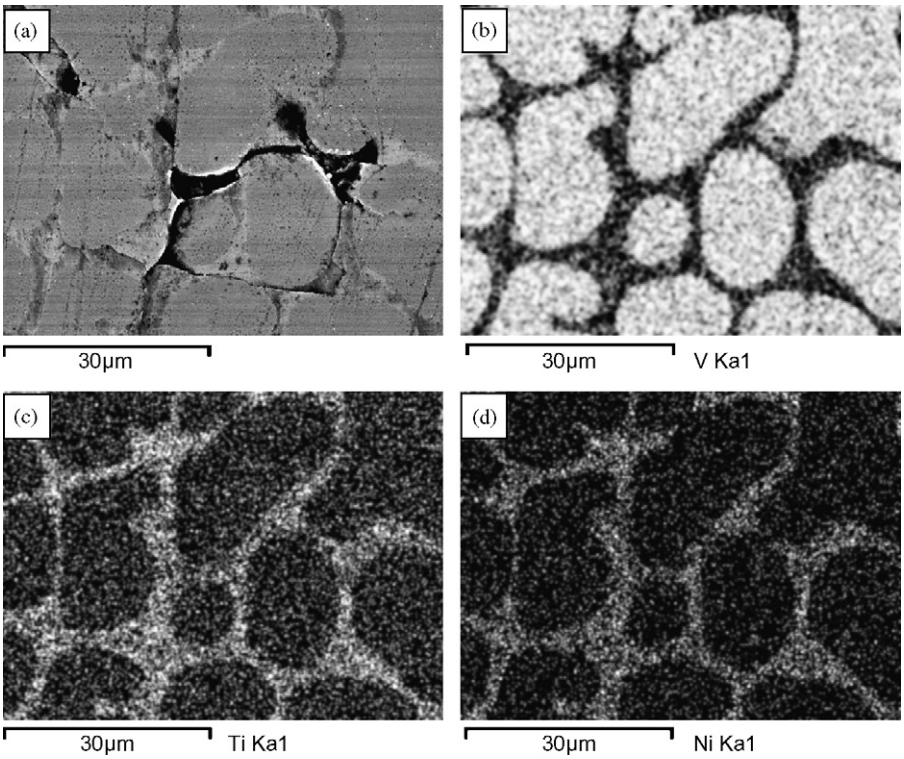

Fig. 3. EDS element maps of the $Ti_{0.8}Zr_{0.2}V_{2.7}Mn_{0.5}Cr_{0.6}Ni_{1.25}Fe_{0.2}$ electrode alloy after the charge/discharge on 108% SOC: (a) the detected area, (b) element V, (c) element Ti, and (d) element Ni.

lager lattice deviation at the interface of the C14 Laves phase and the V-based phase, and finally the interface failed.

Fig. 3(a)–(d) shows the EDS element maps of the $Ti_{0.8}Zr_{0.2}V_{2.7}Mn_{0.5}Cr_{0.6}Ni_{1.25}Fe_{0.2}$ alloy electrode after the charge/discharge process at 144% SOC, of which Fig. 3(a) is the EDS detection area. It can be seen from Fig. 3 that the crack region has higher concentration of Ti and Ni compared with the other elements and the V-based phase is V enrichment, which confirm the element concentration distribution characteristic of the C14 Laves phase and the V-based phase listed in Table 1.

V is one of the hydrogen absorbing elements of the Ti–V-based hydrogen storage electrode alloy. The dissolution of V during cycling is severe [15,16,18]. Fig. 4 is an SEM micrograph of the $Ti_{0.8}Zr_{0.2}V_{2.7}Mn_{0.5}Cr_{0.6}Ni_{1.25}Fe_{0.2}$ alloy after being dipped in a 4 M KOH solution for 720 h stilly. It can be seen clearly that the V-based phase becomes concave and the C14 Laves phase becomes convex, which indicate that the V-based BCC phase is less corrosion-resistant than the C14 Laves phase. Fig. 5(a)–(c) is the surface morphologies of the alloy electrode after discharge which were charged to different state under AFM. It is seen that the surface of the as-prepared sample is very flat, the C14 phase and V-based phase being almost at the same surface level. With the increase of the charge duration, the chromatism between the V-based phase and the C14 Laves phase increases and the color of the C14 Laves phase becomes deeper (from Fig. 5(b) to (c)), which indicate that the surface of the C14 phase is concave compared with that of the V-based phase. That is, the loss of the two phases in the alkaline during charge/discharge process is not only based on their corrosion resistance displayed from the still dip condition. The larger amount of loss of the C14 Laves phase in the charge/discharge process is related to its larger volume expansion/constriction which caused a severer desquamation than the V-based phase. The desquamation of the C14 Laves phase somewhat quickened the crack broadening both in the C14 Laves phase and at the phase boundary.

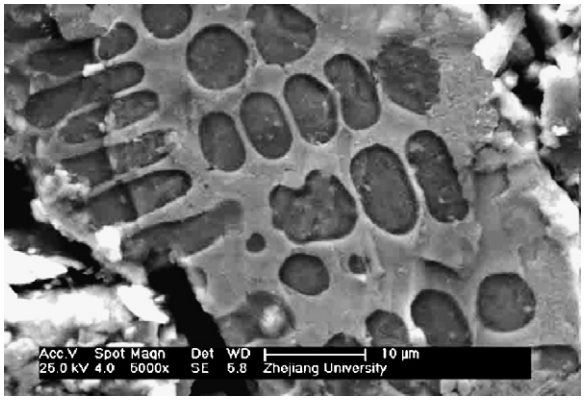

Fig. 4. SEM micrograph of the $Ti_{0.8}Zr_{0.2}V_{2.7}Mn_{0.5}Cr_{0.6}Ni_{1.25}Fe_{0.2}$ alloy being dipped in the 4 M KOH solution for 720 h stilly.

It is also reported by Iba and Akiba [5] that the secondary catalyst phase of TiNi of a Ti–V–Mn hydrogen storage alloy disappeared with the charge/discharge cycling extending to some level, and it is taken as an important factor causing the capacity fading of the alloy electrode. The authors attributed the disappearance of the TiNi phase to its corrosion. The crack-pits in the C14 Laves phase and at the phase boundary in Fig. 1(d)–(f) shows a similar phenomenon of the disappearance of the TiNi phase in their study. But the disappearance of the C14 Laves phase in the present study is mainly attributed to the pulverization of the C14 Laves phase, and the fractured pieces losing the bonding to the matrix. The dissolution and the corrosion of the C14 Laves phase are the secondary. For the usual powder alloy electrode, with the cycling, the pulverized C14 Laves phase is thought to become isolated small pieces, leading to the V-based phase lacking of catalysis from the C14 Laves phase. The increasing contact resistance of the alloy electrode caused by the pulverization for the multiphase Ti–V-based alloys [15,19] should also correlate with the pulverization of the C14 Laves phase or the

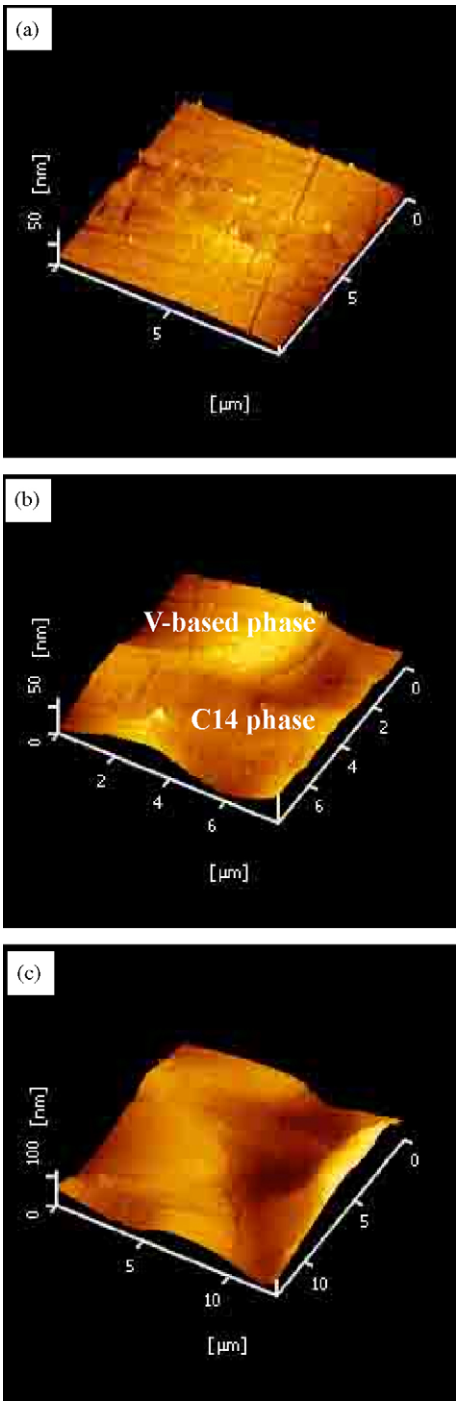

Fig. 5. AFM images of the $Ti_{0.8}Zr_{0.2}V_{2.7}Mn_{0.5}Cr_{0.6}Ni_{1.25}Fe_{0.2}$ alloy (a) and the alloy electrodes after the charge/discharge process on 36% SOC (b), and 108% SOC (c).

TiNi secondary phase. So far, it is reasonable that the pulverization of the C14 Laves phase and its failure of the connecting with the V-based phase play an important role in the degradation of cycle stability.

In the extending study on the purpose of clarifying the correlation between the pulverization behavior of the Ti–V-based alloy and the fracture toughness as well as the hardness of the V-based BCC phase and the C14 Laves phase, it was found that the Vickers hardness of the "C14-based alloy" and "V-based alloy" are of 2.9 and 2.3 GPa, respectively. The former is harder than the latter. The images of the Vickers indentation under the load of 49 N are displayed in Fig. 6. Certainly the indentation size of the "C14-based alloy" is smaller than that of the "V-based alloy". Moreover, there are long indentation cracks in the "C14-based Laves alloy", whereas there is almost no indentation crack in the "V-based" alloy. There is no doubt that the fracture toughness of the "C14-based alloy" is much lower than that of the "V-based alloy". As the XRD analysis of the two alloys (Fig. 7) show that the "V-based alloy" is almost only composed of the V-based BCC phase and the "C14-based alloy" is mainly composed of the C14 Laves phase. As the characteristic peak around 40° in the "C14-based alloy" is relatively smaller than the peak from the typical C14 phases [JCPDS-48-1692/1694/1696], and the main peaks of the C14 Laves phase and C15 Laves are overlapped, it is also possible that the alloy contains small portion of C15 laves phase. The mechanical properties measured from the two alloys presumably represent the mechanical properties of the V-based BBC phase and C14 Laves phase in

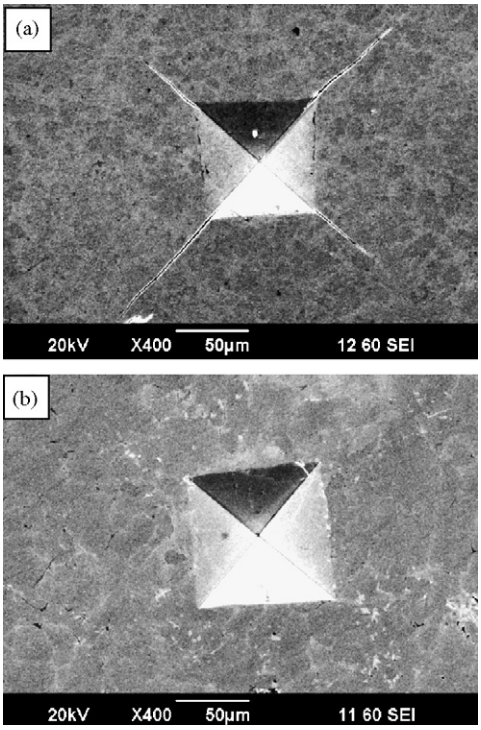

Fig. 6. Images of Vickers indentation of the "C14-based alloy" (a) and the "V-based alloy" (b) under a load of 49 N.

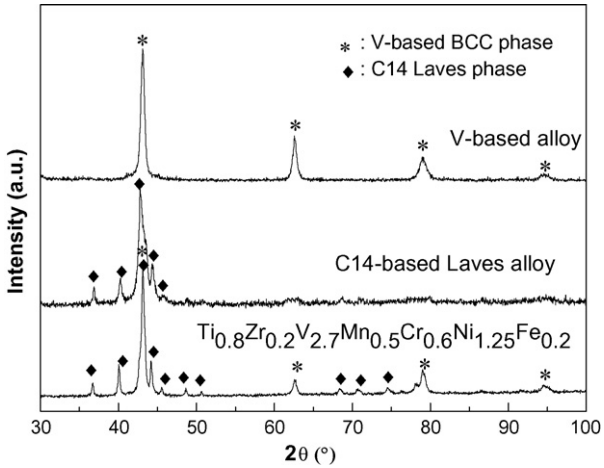

Fig. 7. XRD patterns of the "C14-based alloy", the "V-based alloy" as well as the $Ti_{0.8}Zr_{0.2}V_{2.7}Mn_{0.5}Cr_{0.6}Ni_{1.25}Fe_{0.2}$ alloy.

the Ti–V-based alloy. Therefore, the lower toughness (higher hardness) of the C14 Laves is another important factor that causes its lower pulverization resistance compared with the V-bases phase during charge/discharge cycling, resulting in the microcracks preferentially propagating in the C14 phase when the alloy suffers large volume expansion/constriction. It is also reported in previous literature that the pulverization rate of the Ti–V-based alloy is closely related to its hardness in a correlation of higher hardness causing a severer pulverization [6], and to improve the mechanical strength of the TiNi phase could also improve the cycle stability of the multiphase Ti–V-based solid solution alloy [2].

Decreasing the cell volume expansion of the hydrogen storage phases during hydrogenation and dehydrogenation can reduce the pulverization of the particles in La–Mg–Ni-based alloys [22]. However, as the hydrogenation of the C14 Laves phase in the multiphase Ti–V-based alloy inevitably causes the volume expansion, thus, in addition to finding ways to reduce the volume expansion of the C14 Laves phase, it may be also important to find ways to improve the fracture toughness of the C14 phase and to strengthen the phase boundary to increase the pulverization resistance of the Ti–V-based alloy.

4. Conclusions

The phase boundary of the V-based phase and the C14 Laves phase of the $Ti_{0.8}Zr_{0.2}V_{2.7}Mn_{0.5}Cr_{0.6}Ni_{1.25}Fe_{0.2}$ hydrogen storage alloy is a weak interface, which is composed of an amorphous layer of high Ti segregation with a thickness of 90 nm. During the charge/discharge process, cracks initially formed at the phase boundary and then propagated to the C14 Laves phase with further charging to deep state. Cracks seldom occurred in the V-based BCC phase. The pulverization of the Ti–V-based alloy is mainly caused by the de-bonding of the V-based BCC phase and the C14 Laves phase and the pulverization of the C14 Laves phase. The weak bonding strength of the phase boundary, the low toughness of the C14 Laves phase and the large cell volume expansion/constriction of the C14 Laves phase during the hydrogenated/dehydrogenated process are the main reasons for the easier formation and propagation of the cracks at the phase boundary and in the C14 Laves phase.

Acknowledgement

This work was financially supported by the Program for New Century Excellent Talents in University of China (No. NCET-06-0519) and the National Natural Foundation of China (No. 50631020).

References

[1] E. Akiba, H. Iba, Intermetallics 6 (1998) 461.
[2] M. Tsukahara, K. Takahashi, T. Mishima, A. Isomura, T. Sakai, J. Alloys Compd. 253–254 (1997) 583.
[3] M. Tsukahara, K. Takahashi, T. Mishima, A. Isomura, T. Sakai, J. Alloys Compd. 236 (1996) 151.
[4] M. Tsukahara, K. Takahashi, T. Mishima, T. Sakai, H. Miyamura, N. Kuriyama, I. Uehara, J. Alloys Compd. 226 (1995) 203.
[5] H. Iba, E. Akiba, J. Alloys Compd. 253–254 (1997) 21.
[6] J.S. Yu, S.M. Lee, K. Cho, J.Y. Lee, J. Electrochem. Soc. 147 (2000) 2013–2017.
[7] Q.A. Zhang, Y.Q. Lei, X.G. Yang, Y.L. Du, Q.D. Wang, Int. J. Hydrogen Energy 25 (2000) 977.
[8] S.J. Qiu, H.L. Chu, Y. Zhang, D.L. Sun, X.Y. Song, L.X. Sun, F. Xu, J. Alloys Compd. 471 (2009) 453.
[9] Y.J. Chai, W.Y. Yin, Z.Y. Li, X.B. Zhang, M.S. Zhao, Intermetallics 13 (2005) 1141.
[10] R. Li, H.G. Pan, M.X. Gao, Y.F. Liu, Y.Q. Lei, Q.D. Wang, J. Alloys Compd. 432 (2007) 183.
[11] H. Miao, M.X. Gao, Y.F. Liu, Y. Lin, J.H. Wang, H.G. Pan, Int. J. Hydrogen Energy 32 (2007) 3947.
[12] Y.F. Zhu, H.G. Pan, M.X. Gao, Y.F. Liu, Q.D. Wang, J. Alloys Compd. 348 (2003) 301.
[13] M. Tsukahara, K. Takahashi, T. Mishima, A. Isomura, T. Sakai, J. Alloys Compd. 243 (1996) 133.
[14] Y.F. Zhu, Y.F. Liu, F. Hua, L.Q. Li, J. Alloys Compd. 463 (2008) 528.
[15] Y.F. Liu, H.G. Pan, M.X. Gao, R. Li, Q.D. Wang, J. Phys. Chem. C 112 (2008) 16682.
[16] Y.F. Zhu, H.G. Pan, M.X. Gao, Y.F. Liu, R. Li, Y.Q. Lei, Q.D. Wang, Int. J. Hydrogen Energy 29 (2004) 313.
[17] H.G. Pan, Y.F. Zhu, M.X. Gao, Y.F. Liu, R. Li, Y.Q. Lei, Q.D. Wang, J. Alloys Compd. 370 (2004) 254.
[18] Y.Q. Qiao, M.S. Zhao, M.Y. Li, X.J. Zhu, G.Y. Cao, Scripta Mater. 55 (2006) 279.
[19] N. Kuriyama, M. Tsukahara, K. Takahashi, H. Yoshinagac, H.T. Takeshitaa, T. Sakaia, J. Alloys Compd. 356–357 (2003) 738.
[20] Y.F. Liu, H.G. Pan, M.X. Gao, Y.Q. Lei, Q.D. Wang, J. Alloys Compd. 403 (2005) 296.
[21] Y.H. Xu, C.P. Chen, X.L. Wang, Y.Q. Lei, X.H. Wang, L.X. Chen, Q.D. Wang, Int. J. Hydrogen Energy 32 (2007) 1716.
[22] Y.F. Liu, H.G. Pan, Y.J. Yue, X.F. Wu, N. Chen, J. Alloys Compd. 395 (2005) 291.